Ecotoxicology and Environmental Safety 303 (2025) 119055

Contents lists available at ScienceDirect

Ecotoxicology and Environmental Safety

journal homepage: www.elsevier.com/locate/ecoenv

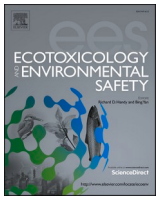

CircSP3 modulates apoptosis and participates in inorganic arsenic carcinogenesis through phosphorylation and ubiquitination of p65

Jinyao Yin [a,b], Qian Zhou [a,c], Chenglan Jiang [a], Shuting Li [a,*], Yuefeng He [a,*]

[a] Yunnan Provincial Key Laboratory of Public Health and Biosafety & School of Public Health, Kunming Medical University, Kunming 650500, China
[b] College of Public Health, Harbin Medical University, 157 Baojian Road, Harbin 150086, China
[c] National Institute of Occupational Health and Poison Control, Chinese Center for Disease Control and Prevention, Beijing, China

ARTICLE INFO

Edited by Tao Zhang

Keywords:
Arsenic
CircSP3
Cell apoptosis
NF-κB
P65

ABSTRACT

Inorganic arsenic (iAs) is a well-established carcinogen known to dysregulate gene expression, but its impact on circular RNAs (circRNAs) remains poorly characterized. Here, we demonstrated that $NaAsO_2$ (20, 40, 60 μmol/L) upregulated circSP3 (hsa_circ_0002642) expression in A549 cells (human lung adenocarcinoma cell line), independent of its methylated metabolites (MMA and DMA). Functionally, circSP3 silencing induced mitochondrial apoptosis, evidenced by reduced Bcl-2/Bax ratio, cytochrome c release, and caspase-7/PARP1 cleavage. Crucially, circSP3 knockdown attenuated NF-κB signaling through ubiquitin-mediated degradation of p65, concomitant with decreased phosphorylation of p65 (Ser536) and IκBα (Ser32/36). RNA immunoprecipitation revealed direct interactions between circSP3 and both p65 and IκBα, with iAs exposure reducing these binding affinities despite increasing circSP3 abundance. Collectively, our findings identify circSP3 as an iAs-responsive regulator of NF-κB-driven survival via post-translational control of p65 stability, providing mechanistic insights into iAs carcinogenesis.

1. Introduction

Arsenic is ubiquitously distributed in environmental matrices, such as the soil, rocks, the lithosphere, hydrosphere, and atmosphere (Pullella and Kotsopoulos, 2020). Classified as a GroupIhuman carcinogen by the International Agency for Research on Cancer, arsenic - particularly its inorganic forms (iAs)-exhibits substantially higher toxicity than organic species (Zheng et al., 2021). Chronic iAs exposure is epidemiologically associated with multiorgan pathologies (Naujokas et al., 2013), constituting a critical global health burden as recognized by the World Health Organization (WHO, 2010). Ingestion of iAs is epidemiologically associated with diverse malignancies, including hepatocellular carcinoma (Lamm et al., 2021), kidney (Ali et al., 2020) and lung cancer (Minna et al., 2011), and pulmonary adenocarcinoma (Kuo et al., 2022). Following absorption, pentavalent iAs (V) can be rapidly reduced to trivalent iAs (III). Hepatic metabolism converts iAs into methylated derivatives (monomethylarsonic acid, MMA and dimethylarsinic acid, DMA), which undergo renal elimination. Residual iAs can be accumulated through the nails, skin and hair (Ali et al., 2012, 2013). Although arsenic metabolism has been correlated with different health outcomes (Wu et al., 2021), MMA and DMA exhibit significantly lower toxicity than iAs (III). Proposed oncogenic mechanisms include induction of oxidative stress, DNA repair impairment, chromosomal aberrations, and epigenetic dysregulation (Ali et al., 2016). To date, with continuous in-depth research on iAs, emerging evidences further implicate iAs in dysregulating circular RNAs (circRNAs), which modulate proliferative/apoptotic balance to promote tumorigenesis, as demonstrated for circRNA 100284 (Dai et al., 2018) and circRNA 008913 (Xiao et al., 2018), etc.

CircRNAs constitute a class of covalently closed, single-stranded RNA molecules lacking canonical 5′-3′ polarity and polyadenylated tails (Hossain et al., 2022). Their expression exhibits pronounced tissue and cell-type specificity, conferring exceptional stability and functional specificity (Li et al., 2022). Compelling evidence indicates that circRNAs modulate fundamental biological processes notably cell cycle progression, proliferation, apoptotic regulation, and metastatic behavior across diverse malignancies (Jeck and Sharpless, 2014). Mechanistically, circRNAs operate through sponging adsorption of microRNAs (miRNAs) (Hansen et al., 2013; Ji et al., 2024), protein translation (Yang et al., 2018; Zhang et al., 2018) as well as direct interactions with signaling proteins (Du et al., 2016; Wang et al., 2021). These multifaceted roles establish circRNA is of great significance in cancer initiation and

* Corresponding authors.
E-mail addresses: lishuting333@126.com (S. Li), heyuefeng@kmmu.edu.cn (Y. He).

https://doi.org/10.1016/j.ecoenv.2025.119055
Received 19 May 2025; Received in revised form 10 September 2025; Accepted 10 September 2025
Available online 13 September 2025

progression. Nevertheless, the significance of hsa_circ_0002642 (circSP3), a circRNA of specificity protein 3 (SP3), remains unclarified in iAs-induced malignancies.

Sp3, a member of the Sp/Krüppel-like factor (Sp/KLF) transcription factor family, coordinates fundamental processes including cellular proliferation, differentiation, apoptosis, and oncogenic transformation (Chen et al., 2020). While paralogs such as Sp1 and Sp4 exhibit overlapping functions, Sp3 demonstrates unique regulatory roles in malignancy. The circSP3, first characterized in 2021, drives hepatocellular carcinoma (HCC) progression through miR-198 sequestration and consequent CDK4 (cyclin-dependent kinase 4) upregulation (Li et al. 2021). Nevertheless, there are two critical knowledge gaps persist. Whether arsenic exposure modulates circSP3 expression, and how circSP3 mechanistically interfaces with iAs-induced carcinogenesis.

As a result, this study aimd to determine whether iAs exposure dysregulated circSP3 expression and elucidate the functional consequences of circSP3 modulation on apoptosis during iAs-induced malignant transformation. Moreover, we also delineated the underlying molecular mechanisms linking circSP3 to iAs carcinogenesis. Using human lung adenocarcinoma (A549) cells as a model system, we provided mechanistic insights into circSP3's role as a potential mediator of iAs toxicity and provided a novel molecular basis for arsenic-associated carcinogens.

2. Materials and methods

2.1. Cell culture

A549 cells were obtained from Cell Bank of the Chinese Academy of Sciences and routinely maintained in RPMI-1640 medium with 10 % (v/v) fetal bovine serum (FBS) and 1 % penicillin-streptomycin. All A549 cells were maintained at 37℃ inside a sterile, humidified space with an atmosphere composed of 95 % air and 5 % CO_2. Change the medium every 2 days.

2.2. Cell Treatment with $NaAsO_2$

2.5×10^5 cells/well were seeded in 6-well plates and allowed to adhere for 22 h. Subsequently, the cells underwent treatment with various concentrations of $NaAsO_2$ (0, 20, 40, 60 μmol/L) as well as 60 μmol/L MMA and DMA (Yin et al., 2022). After incubation for 48 h, the total RNA was extracted and used in subsequent experiments.

2.3. RNA isolation and quantitative real-time PCR (Q-PCR)

Total RNA was extracted using TRIzol Reagent from A549 cells in line with the manufacturer's guidelines. The synthesis of cDNA was performed with 1 μg total RNA using the HiFiScript cDNA Synthesis Kit (CoWinBiotech). Quantitative PCR amplification utilized SYBR® Green PCR Master Mix (CoWin Biotech) on a LightCycler® 96 System (Roche), as previously described (Yin et al., 2022). All samples were run in triplicate with β-actin as the endogenous control and data was analyzed by $2^{-\Delta\Delta Ct}$ approach. Primer sequences:

CircSP3 Forward: ACTTTGACGCCTGTTCAAACC
CircSP3 Reverse: AAGCCAAATCACCTGTCTGCAG
β-actin Forward: CCCTGTACGCCAACACAGTGC
β-actin Reverse: ATACTCCTGCTTGCTGATCC

2.4. Cell transfection

A549 cells in logarithmic growth stage were plated into cell plates at 35–55 % conflence using RPMI 1640 medium that included 10 % FBS, and cultured in the 37 °C, 5 % CO_2 incubator for 19 h. Subsequently, transfection was performed using RFect™ Reagent conforming to the manufacturer's rule and continued culture. Experimental groups included the negative control (NC) group and the siRNA targeting circSP3 group (si-circSP3). Transfection efficiency was monitored using fluorescence microscopy at 6 h post-transfection. Cells were harvested at 72 h for subsequent experiments, such as Q-PCR, western blot, etc. SiRNA sequences are presented as follows:

NC Forward: UUCUCCGAACGUGUCACGUTT
NC Reverse: ACGUGACACGUUCGGAGAATT
si-circSP3 Forward: AGUCCUGCAGACAGGUGAU
si-circSP3 Reverse: AUCACCUGUCUGCAGGACU

2.5. Cell viability assay

Cell Counting Kit-8 (CCK-8) assay was employed to detect the A549 cell viability, according to the manufacturer's protocols. Briefly, logarithmic growth stage A549 cells (2500 cells/well with 100 μl) were plated in 96-well plates. After silencing treatment for 72 h, 10 μL CCK-8 reagent was added to each well followed by 1 h incubation at 37 °C. Subsequently, the absorbance was measured using a microplate reader at 490 nm.

2.6. Mitochondrial membrane potential analysis (JC-1 staining)

JC-1 staining was utilized to inspect the variation of mitochondrial membrane potential (MMP). A549 cells were plated into 96-well black plates at 2500 cells/well. Following transfection for 72 h, the media were removed, then cells were stained with the JC-1 reagent (60 μL/well) and underwent incubation for 20 min at room temperature in dark. After the mixture was abandoned, the stained cells were washed twice using 200 μL ice-cold PBS (phosphate-buffered saline) per well. Subsequently, 60 μL ice-cold PBS was added to each well to examine the alterations in MMP. JC-1 aggregates in the mitochondria were detected by red fluorescence (550 nm, 600 nm). The cytoplasm JC-1 monomers were detected by green fluorescence (485 nm, 535 nm). The reduction of red/green fluorescence intensity was considered to an early sign of apoptosis.

2.7. Cell apoptosis assay

Apoptosis was quantified using the Hoechst 33342/PI (propidium iodide) Dual Stain Kit. A549 cells were plated in 6-well plates at 8×10^4 cells/well. After 72 h transfection, the cells underwent two washes with PBS and added into Hoechst 33342 and PI reagent for 15 min at room temperature protected from light. Following three PBS washes, next added 600 μL/well PBS to image under an inverted fluorescence microscope.

2.8. Protein isolation and Western blotting

Cells were lysed in RIPA buffer for 20 min at 4℃. The protein concentration was determined by means of the BCA Protein Assay kit. The proteins were then separated utilizing SDS-PAGE electrophoresis and transferred to polyvinylidene fluoride (PVDF) membranes. After that, the PVDF membranes were blocked for 20 min at room temperature and maintained with primary antibodies overnight at 4℃. After TBST washes, the membrane was maintained with secondary antibodies for 2 h, and afterwards, was washed three times employing PBS. Before imaging, PVDF membranes stored in PBS. Proteins were visualized using BeyoECL™ Plus and imaged with the Gel-Pro Analyzer software. Band intensities were quantified using ImageJ with β-actin normalization.

2.9. Co-immunoprecipitation assays (Co-IP)

A549 cells (1.3×10^6 cells/dish) were transfected and harvested after 72 h. Then, cells were broken down with RIPA buffer containing protease/phosphatase inhibitors. Total protein was extracted and incubated with corresponding antibodies on the incubated rotor overnight at 4℃. Following this, Antibody-protein complexes were captured by Protein

A/G Magnetic Beads (pre-blocked with 5 % BSA for 1 h) for 6 h at 4°C. Beads were washed three times with PBST, the combination sample was resuspended in the 1 ×loading buffer and immediately denatured at 95°C for 5 min. Denatured proteins were detected by western blot assay according to the described above.

2.10. RNA binding protein immunoprecipitation assay (RIP)

1.7×10^6 cells were seeded into culture dishes. Following culture for 24 h, cells underwent additional treatment with 40 μmol/L $NaAsO_2$ for another 48 h. The total protein isolated from A549 cells was dissolved in equal amounts of antibodies, and then immediately incubated on the rotor for a night at 4℃. Following this, the magnetic beads (25 μl) sealed for 1 h were mixed with the antigen-antibody complex and agitated at 4℃ for 5 h 20 min. After washing (three times, with PBST), RNA extraction was performed as described in the above experimental steps.

2.11. Statistical analysis

All experiments were replicated independently a minimum of three times. Data analysis was conducted with the SPSS 22.0, GraphPad Prism 6.0 and ImageJ software. The statistical analysis for experimental data was carried out via Student's t - test or χ^2. The outcomes were presented as mean ± standard deviation (SD). If $P < 0.05$, it was deemed to represent a statistically significant difference.

3. Results

3.1. $NaAsO_2$ promoted the expression of circSP3 within A549 cells but DMA, MMA had no effect on circSP3

To investigate whether circSP3 is involved in the carcinogenic process of iAs, we examined the effects of DMA, MMA and a range of concentrations of $NaAsO_2$ (0, 20, 40, 60 μmol/L) on the expression of circSP3 in A549 cells using Q-PCR. Similar to the other genes we described earlier (Tan et al., 2022), exposures of A549 cells to $NaAsO_2$ promoted the expression of circSP3 **(**Fig. 1**A)**. With $NaAsO_2$ exposure concentration increases, the tendency of circSP3 expression upregulation grew increasingly apparent. On the contrary, neither MMA nor DMA (60 μmol/L) altered circSP3 expression **(**Fig. 1**B)**.

3.2. Knockdown of circSP3 in A549 cells

Transfected A549 cells with the RFect reagent did not alter cellular morphology or proliferation (Fig. 2A), confirming its biocompatibility for downstream applications. Following the Q-PCR results, the circSP3 expression in the si-circSP3 group was markedly decreased (Fig. 2B). In contrast, SP3 mRNA levels remained unchanged (Fig. 2C), validating the si-circSP3 specifically targets hsa_circ_0002642 and successfully knocks down the circSP3.

3.3. Knockdown of circSP3 significantly promoted apoptosis of A549 cells

CircSP3 knockdown significantly reduced cell viability (Fig. 3A) and decreased MMP (Fig. 3B). To further confirm the involvement of circSP3 in apoptosis and proliferation, Hoechst 33342/PI staining experiments were performed. We observed extensive cell apoptosis in the si-circSP3 group, following results in Fig. 3C. Morphological analysis revealed chromatin condensation and nuclear fragmentation in si-circSP3 cells.

3.4. Knockdown of circSP3 affected apoptosis-related proteins

According to the above results, circSP3 with low expression significantly reduced MMP, suggesting that apoptosis was closely related to mitochondrial pathway. In order to further verify the impact of circSP3 on apoptosis of A549 cells, Western blot analysis was utilized to assess the expression of mitochondrial apoptosis-related proteins (Bcl-2, Bax, Cytc, caspase7, and PARP1). The outcomes showed that in comparison with the NC group, the expression of Bcl-2 protein in the si-circSP3 group was considerably decreased, whereas the expression of Bax, Cytc, Cleaved caspase7 and Cleaved PARP1 were significantly increased (Fig. 4A). The Bcl-2/Bax ratio decreased in the si-circSP3 group (Fig. 4B). These changes demonstrated that circSP3 silencing initiated caspase-dependent apoptosis through Bax-mediated mitochondrial permeabilization.

3.5. Co-culture Incubation A549 cells with si-cirSP3 and $NaAsO_2$, and the apoptosis was more obvious

To delve deeper into the impact of circSP3 on apoptosis and proliferation in the presence of iAs, we added an appropriate amount of $NaAsO_2$ to the cells 24 h after transfection, so that the final concentration of $NaAsO_2$ was 40 μmol/L, and continued culture for 48 h. Subsequently, cell apoptosis was determined using CCK-8 assay, JC-1 assay and Hoechst33342/PI assay. Combinatorial treatment with si-circSP3 and 40 μmol/L $NaAsO_2$ synergistically enhanced apoptotic signaling versus single interventions (Fig. 5A–C). Collectively, these outcomes indicated that with the existence of $NaAsO_2$, the apoptosis was more obvious in the si-circSP3 group. This synergy underscored circSP3 as a key modulator of arsenic toxicity responses.

3.6. Knockdown of circSP3 inhibited the activity of the p65 pathway

An endeavor to comprehend the molecular mechanism of circSP3 in

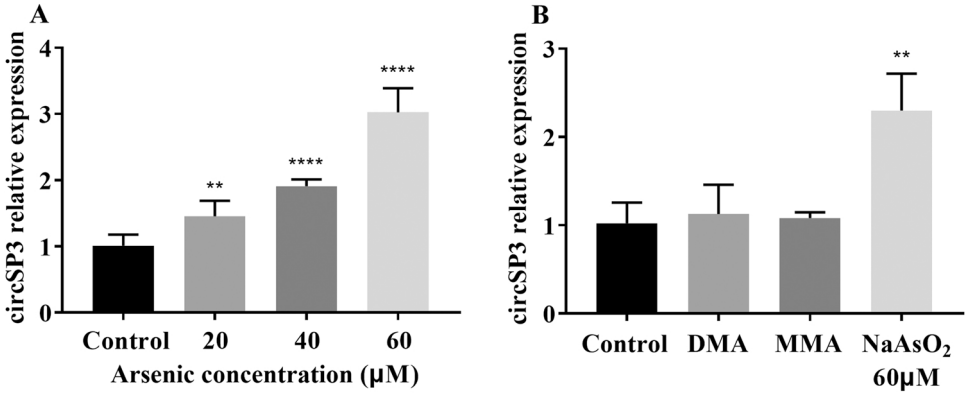

Fig. 1. Effects of $NaAsO_2$, DMA and MMA on circSP3 expression in A549 cells (in comparison to the control group, **P < 0.01, **** P < 0.0001). (A) Effects of different concentrations of $NaAsO_2$ (0, 20, 40, 60 μmol/L) on the relative expression of circSP3. (B) Effects of DMA (60 μmol/L) and MMA (60 μmol/L) on the relative expression of circSP3.

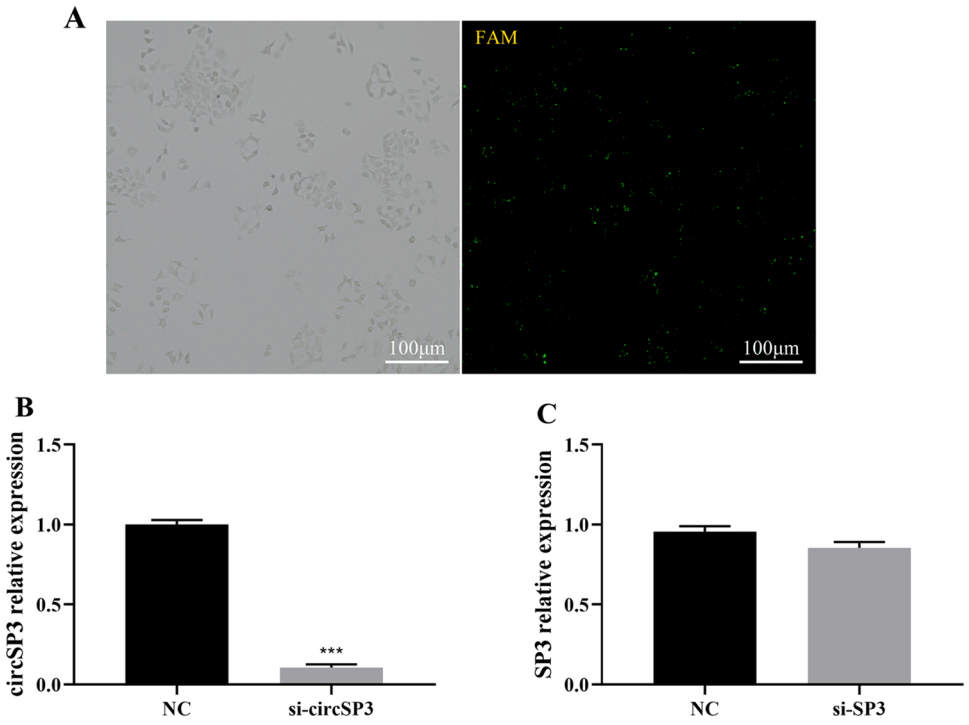

Fig. 2. Specific silencing targeting circSP3. (A) Transfection efficiency of RFect reagent. (B and C) Silence circSP3, circSP3 and SP3 relative expression levels (In comparison to the control group, ***P < 0.001).

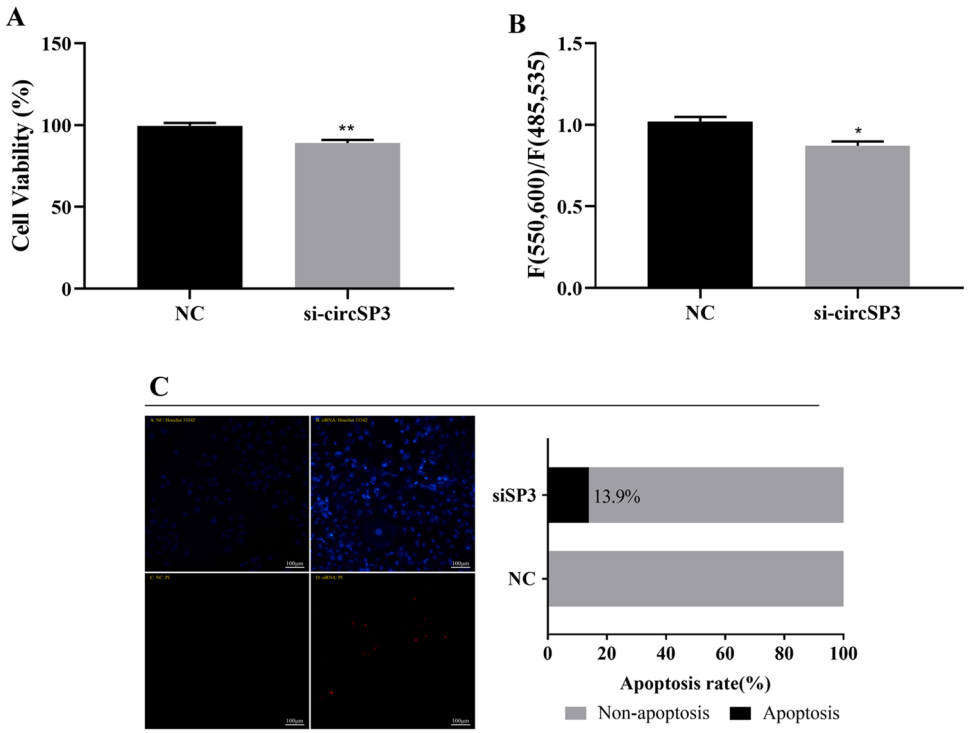

Fig. 3. Changes of cell viability, mitochondrial membrane potential and apoptosis before the silencing of circSP3 and after it. (In comparison to the control group, *P < 0.05, **P < 0.01). (A) CCK-8 assay was employed to measure the influence of circSP3 silencing on cell viability. (B) JC-1 test detected changes of mitochondrial membrane potential after circSP3 silence. (C) The apoptosis of NC group and si-circSP3 group was inspected with a fluorescence microscope and count the apoptotic cells and calculate the apoptotic rate.

regulating apoptosis of A549 cells. After transfection for 72 h, protein was extracted and western blot analysis were performed to observe the alterations of circSP3 with low expression on p65 signaling pathway related proteins. The findings indicated that in comparison to the NC group, the protein expressions of p65, c-IAP1, XIAP and Bclx in si-circSP3 group were significantly decreased, while p21 was significantly increased (Fig. 6A). All changes were quantitatively analyzed by ImageJ and were statistically significant (Fig. 6B). In addition, the

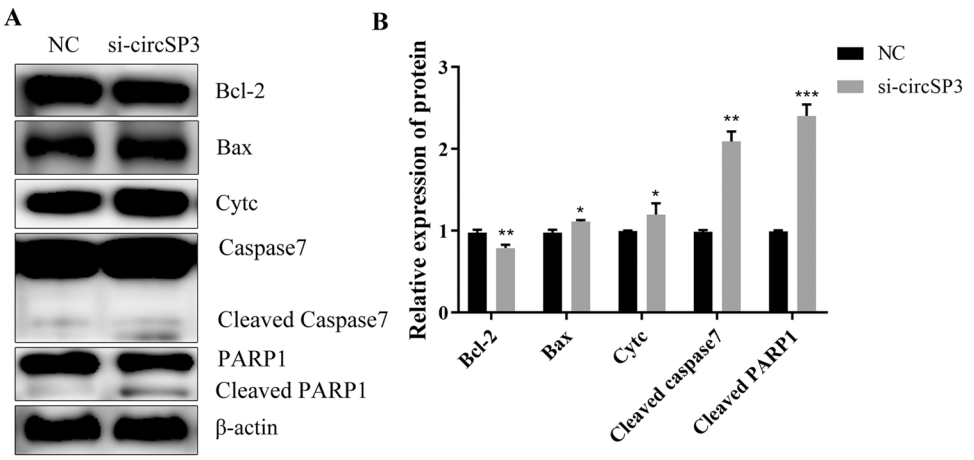

Fig. 4. Western blotting assay targeting apoptosis - associated proteins in cells with silenced circSP3 (compared with control group, *P < 0.05, **P < 0.01, *** P < 0.001) (A) Western blot was employed to measure the alterations of apoptosis-related proteins silencing circSP3. (B) Calculate the gray value of silencing circSP3 apoptosis-related proteins.

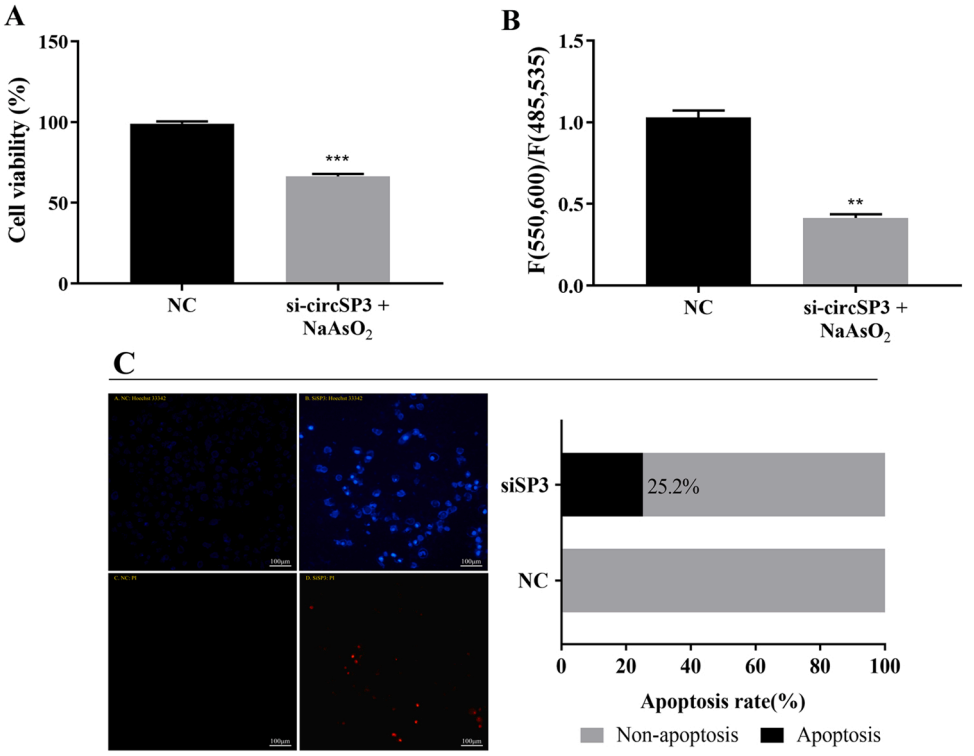

Fig. 5. Co-culture Incubation A549 cells with si-cirSP3 and $NaAsO_2$, changes in cell apoptosis (compared with control group, **P < 0.01, *** P < 0.001). (A) CCK-8 assay was applied to detect the changes of cell viability after $NaAsO_2$ and si-circSP3 were treated together. (B) JC-1 test detected the changes of mitochondrial membrane potential after $NaAsO_2$ and si-circSP3 were treated together. (C) The apoptosis of cells in the two groups was inspected through an inverted fluorescence microscope.

protein expressions of p65 phosphorylated at Ser536, IκBα, IκBα phosphorylated at Ser32 and IκBα phosphorylated at Ser36 were down-regulated in the si-circSP3 group, $p < 0.05$ (Fig. 6C, D). Yet, a substantial increase was noted in p65 ubiquitylation (Fig. 6E).

3.7. Interaction of circSP3 with p65 and IκBα

To explore the relationship between circSP3 and p65, we carried out RIP experiments and found that there was an obvious combination between p65 and circSP3, and it was unexpectedly found that circSP3 could also bind to IκBα (Fig. 7A). It has been extensively reported that IκBα can bind to p65. Hence, we silenced circSP3 to observe the change of the binding force of IκBα with p65, and found that the binding of IκBα with p65 was significantly reduced in si-circSP3 group (Fig. 7C).

3.8. $NaAsO_2$ reduced the binding of circSP3 to p65 protein and IκBα protein, respectively

The above experimental results have proved that $NaAsO_2$ can promote the expression of circSP3. To further explore whether $NaAsO_2$ can affect the binding of circSP3 and p65, 0 and 40μmol/L $NaAsO_2$ were applied to A549 cells for 48 h, respectively, and then RIP experiment

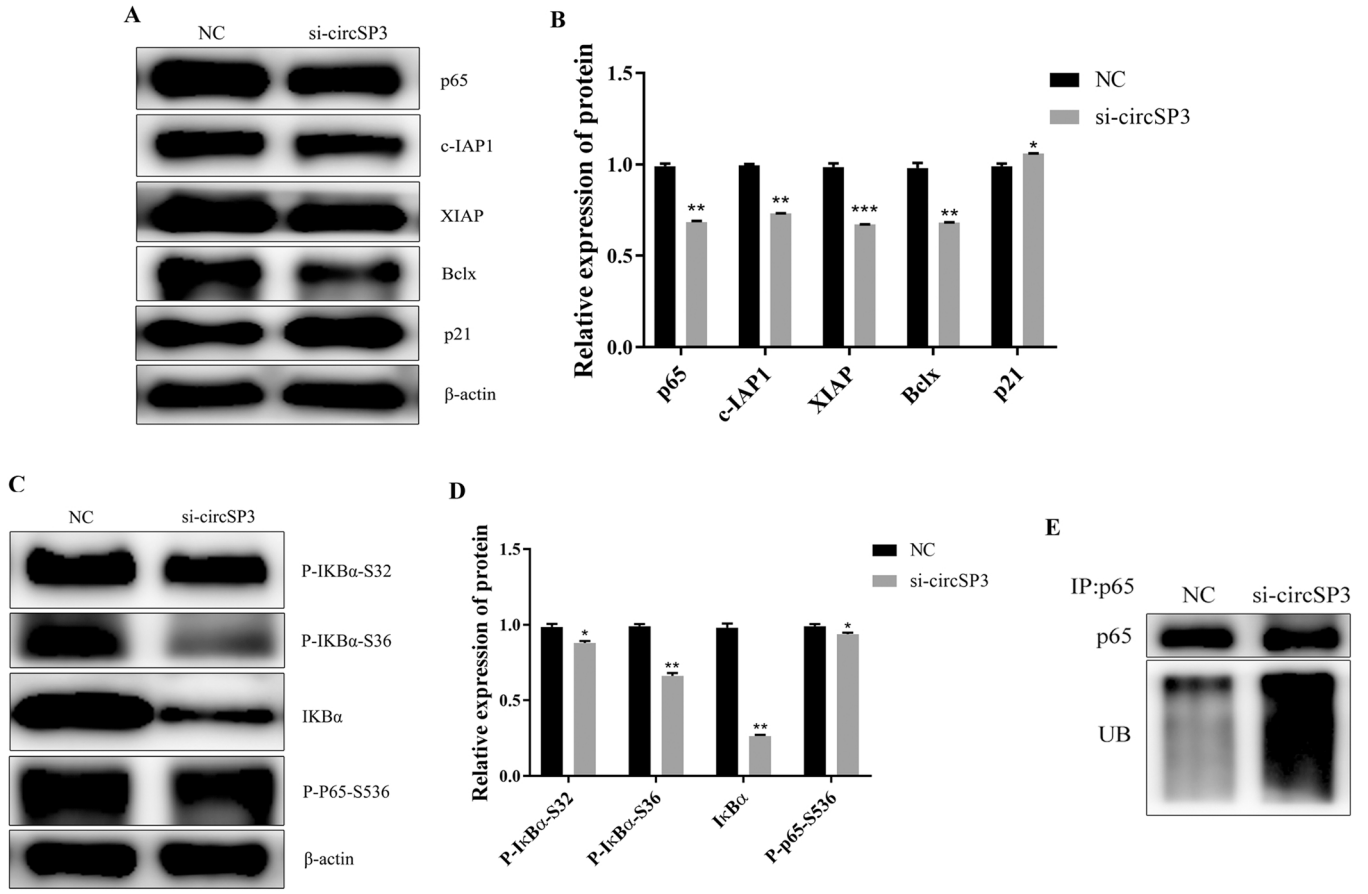

Fig. 6. Influence of circSP3 silencing on protein expression levels (as compared to the control group, *P < 0.05, **P < 0.01, *** P < 0.001). (A) Western blot assay was employed to measure the effect of silencing circSP3 on the expression of p65 and its downstream protein. (B) Calculate the gray value of silenced circSP3 on p65 and its downstream proteins. (C) The impact of suppressing circSP3 on the expression of IκBα, p65 and their phosphorylation. (D) The statistical relevance of the effect of silencing circSP3 on the expression of IκBα, p65 and their phosphorylation was calculated using gray values. (E) Effect of silencing circSP3 on p65 ubiquitination.

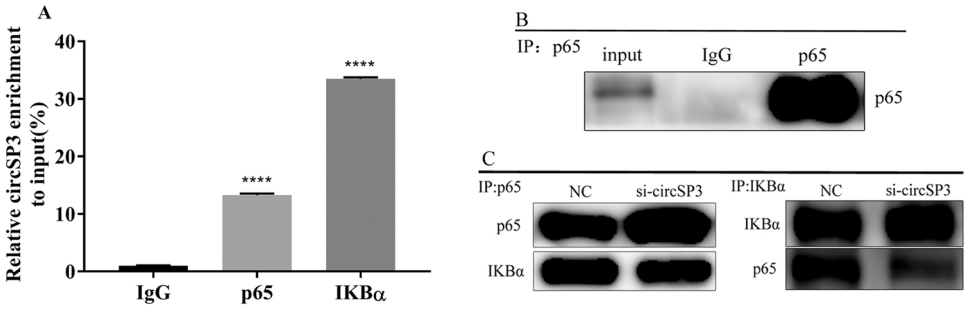

Fig. 7. Binding of circSP3 to p65 and IκBα. (A)Association of circSP3 with p65 and IκBα (compared with control group, ****P < 0.0001). (B) Prove the success of Co-IP experiment; (C) The binding force between circSP3, p65 and IκBα was significantly reduced by silencing.

was performed. RIP protein was divided into two groups. The first group was loaded into corresponding Loading, boiled at 95℃ and placed in the refrigerator at −20℃ for subsequent western blot experiments. The other set was used for normal RIP experiments. In western blot assay, IκBα was used as the internal reference. The IκBα in the group serving as a control and the $NaAsO_2$ group was adjusted (Fig. 8A). Subsequently, the above adjusted dose of IκBα protein was converted, and the binding of circSP3 to p65 was detected by Q-PCR when the IκBα was consistent in the two groups. The outcomes revealed that under the premise of consistent IκBα, the binding of circSP3 to p65 was markedly decreased in the $NaAsO_2$ group, and the variation was statistically meaningful (P < 0.05) (Fig. 8B).

We suspected that $NaAsO_2$ might also affect circSP3 binding to IκBα protein. To verify the hypothesis, we similarly treated A549 cells with 0 and 40 μmol/L $NaAsO_2$ and performed RIP experiments. Similarly to the above methods, in the western blot experiment, p65 was used as the internal reference to make the p65 protein band strength consistent between the control group and the $NaAsO_2$ group (Fig. 8C). Subsequently, the above p65 protein doses were converted and subsequently Q-PCR experiments were carried out. The results showed that under the premise of consistent p65, the binding of circSP3 and IκBα also decreased significantly in the $NaAsO_2$ group, with statistical significance (Fig. 8D).

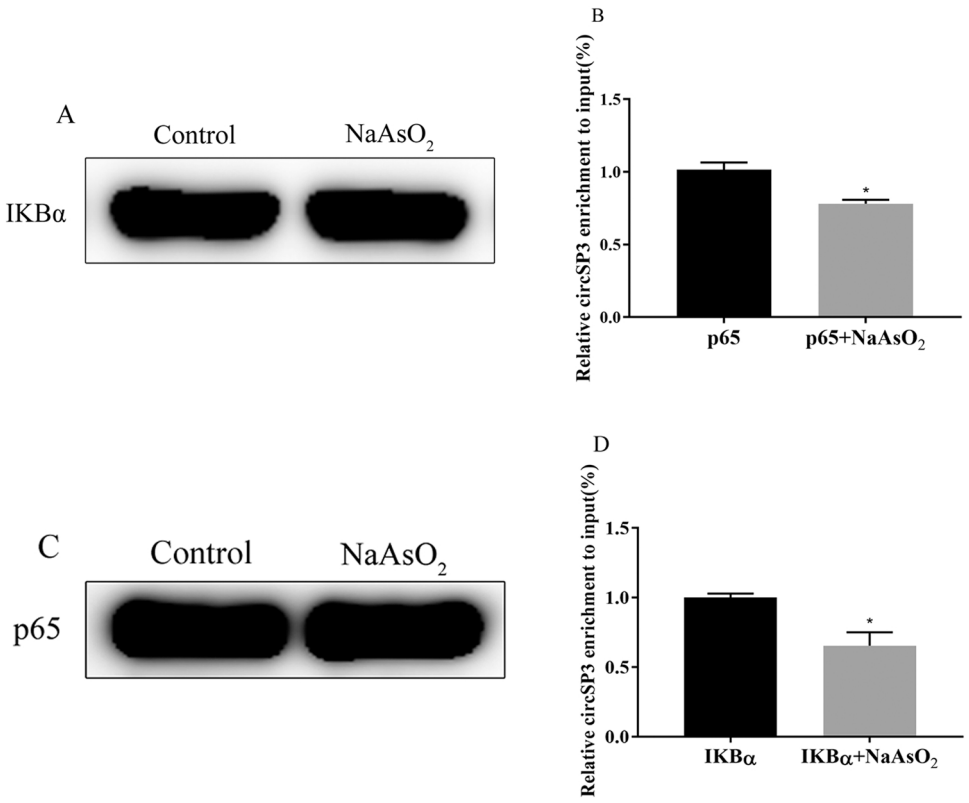

Fig. 8. Influence of $NaAsO_2$ on circSP3 binding to p65, IκBα protein (compared with control group, *P < 0.05).(A)Western blot assay adjusted the IκBα protein of the two groups. (B) The effect of iAs on the binding ability of p65 protein to circSP3 after the adjustment of IκBα was detected by Q-PCR. (C) Western blot test adjusted p65 protein of the two groups. (D) The effect of iAs on the binding ability of IκBα protein to circSP3 after p65 adjustment was detected by Q-PCR.

4. Discussion

Chronic iAs exposure is associated with multiorgan pathologies (Salmeri et al., 2020), and significantly elevates malignancy risk across multiple tissue types. Growing evidence indicates that the carcinogenic mechanisms of iAs including interference of gene expression, oxidative DNA damage (Kojima et al., 2009), regulation of cell proliferation and induction of apoptosis (Medda et al., 2021). In addition, extensive studies have shown that iAs entering the body is eventually metabolized into MMA and DMA after a series of oxidative methylation reactions and eliminated via renal excretion. Notably, both MMA and DMA demonstrate oncogenic potential in human systems. The transcription factor SP3, commonly overexpressed in malignancies, is tightly regulated during tumor initiation and progression (Liu et al., 2021; Safe, 2023). Consequently, our study aimed to examine whether circSP3 had a similar effect in A549 cells, that was, to participate in cell proliferation or apoptosis, and to study the effect of iAs on circSP3 expression as well as the possible molecular mechanism of circSP3 in iAs-induced carcinogenesis.

Here, we investigated the comparative expression level of circSP3 in A549 cells treated within MMA, DMA and different concentrations of $NaAsO_2$, respectively. We observed that different concentrations of $NaAsO_2$ all promoted the expression of circSP3. This iAs-specific induction aligned with established evidence that arsenic exposure dysregulated circRNAs in carcinogenesis, as demonstrated when arsenic-induced circ100284 overexpression promoted malignant transformation (Dai et al., 2018). Crucially, the differential response to iAs versus its metabolites (MMA and DMA) suggested iAs and its methylated metabolites had significant differences in their effects on gene expression, which might lead to differences in their carcinogenic potential. This observation aligned with previous research (Tan et al., 2020).

Substantial evidence has indicated iAs and SP3 regulated apoptosis, proliferation and malignant transformation (Li et al., 2011; Park et al., 2015). Further, iAs exposure can cause abnormal aberrant gene expression and signaling pathway alterations (Dai et al., 2018; Xue et al., 2017). To explore whether circSP3 participated in these processes, we specifically knocked down circSP3 by means of siRNA. Next, cell viability and apoptosis assays revealed that as compared with the NC group, cell vitality and MMP of the si-circSP3 group were noticeably decreased, and cell apoptosis was obvious. These findings aligned with circSP3's documented role in HCC, where its downregulation promoted apoptosis. To verify these observations, we further analyzed apoptosis-related proteins. B-lymphoblastoma-2 (Bcl-2), a critical MMP regulator, maintained MMP homeostasis in the mitochondrial apoptosis pathway.

The Bcl-2 family includes two types of proteins, and the stoichiometric balance between these subsets determines cellular fate (Kale et al., 2017), one is anti-apoptotic protein such as Bcl-XL, Bcl-W, etc, and the other is pro-apoptotic protein such as Bax, Bad, etc. Bcl-2 family proteins are related regulators of apoptotic cell death(Adams and Cory, 2017; Czabotar et al., 2013; Singh et al., 2019). As central regulators of apoptosis, we observed significantly reduced Bcl-2 expression with concurrent increases in Bax, Cytc, caspase7, Cleaved caspase7, and Cleaved PARP1. Bax/Bcl-2 dysregulation triggered the activation of caspase and PARP, key inducers of apoptosis (Chen et al., 2021). Crucially, caspase activation is a central event in the mitochondrial apoptotic pathway (Bock and Tait, 2019). Cleavage of PARP1, a significant caspase substrate, serves as a hallmark apoptotic indicator (Chen et al., 2022). Collectively, these findings suggested that silencing circSP3 triggered caspase-dependent apoptosis via mitochondrial pathway. We next examined whether circSP3 downregulation potentiated $NaAsO_2$-induced apoptosis. Co-treatment of A549 cells with si-cirSP3 and $NaAsO_2$ resulted in significantly enhanced apoptosis compared to controls, indicating that circSP3 could mediate the

abnormal apoptosis or proliferation of cells induced by $NaAsO_2$.

The anti-apoptotic protein Bcl-2 serves as a target gene for NF-κB/p65 and contributes to NF-κB-mediated suppression of apoptosis (Chen et al., 2021; Dang et al., 2020). Given this regulatory link, we detected the changes of p65 and its key downstream gene proteins before and after circSP3 silencing. P65, a major transactivating subunit of NF-κB, plays a pivotal role in regulating cellular survival pathways (Beauchef et al., 2012; Mao et al., 2022). Specifically, modulation of p65 activity is a critical event in NF-κB signal transduction (Wang et al., 2016). Following circSP3 knockdown, we demonstrated a significantly decrease in the protein levels of p65, c-IAP1, XIAP and Bclx. Conversely, p21 expression was markedly increased. Notably, Bclx, XIAP, c-IAP1 and p21, are established transcriptional targets of NF-κB. (Ahn et al., 2007; Ghantous et al., 2012; Takada et al., 2005). Collectively, these findings proved that circSP3 knockdown attenuated the NF-κB signaling axis.

Post-translational modifications like phosphorylation, acetylation, methylation, and ubiquitination, critically regulate the transcriptional activity and function of p65, thereby influencing diverse physiological and pathological processes, including inflammation, immune responses, cell death, proliferation, differentiation, and tumorigenesis (Sun et al., 2024). Among these post-translational modifications, phosphorylation is a principal mechanism for regulating p65 activity. To date, 12 phosphorylation sites (9 serine and 3 threonine residues) have been identified on p65 (Hochrainer et al., 2013; Viatour et al., 2005). Notably, Ser536 undergoes phosphorylation by various kinases, for example, IκB kinases and ribosomal subunit kinase-1 (RSK1), in response to various stimuli (Adli and Baldwin, 2006; Buss et al., 2004). Crucially, our data revealed that the protein levels of phospho-IκBα (Ser32/Ser36), IκBα and P-P65-S536 in si-circSP3 group was notably reduced, while concomitantly increasing p65 ubiquitination. Based on these findings, we speculated that circSP3 silencing reduced p65 abundance primarily by inhibiting its phosphorylation and promoting its ubiquitination (Yang et al., 2003) This reduction in p65 subsequently attenuated the phosphorylation of IκBα at S32 and S36, leading to the diminished IκBα degradation and thus increased IκBα protein levels.

To delineate the mechanistic relationship between circSP3 and the NF-κB complex, we conducted RIP experiments. These experiments revealed direct binding between circSP3 and both p65 and IκBα. While the p65-IκBα interaction is well-established (Fan et al., 2009), the circSP3-IκBα association represents a novel finding. We therefore investigated the binding ability of p65 and IκBα by using Co-IP assay by knockout circSP3. Notably, circSP3 knockdown significantly attenuated the p65-IκBα interaction. We posited that this reduced binding primarily stemmed from diminished p65 and IκBα protein abundance upon circSP3 silencing, consistent with our earlier observations.

5. Conclusion

In summary, our study provided the first demonstration that iAs and its principal methylated metabolites regulated circSP3 expression. We further established that circSP3 served as a critical effector in iAs-driven carcinogenesis, where it potentiated malignant transformation by disrupting the p65/IκBα signaling axis via enhanced ubiquitin-mediated degradation. These findings elucidated a previously unrecognized circRNA-dependent mechanism of iAs toxicity and offered novel therapeutic targets for iAs-associated malignancies.

CRediT authorship contribution statement

Jinyao Yin: Writing – review & editing, Writing – original draft, Data curation. **Chenglan Jiang:** Supervision. **Qian Zhou:** Supervision, Investigation. **Shuting Li:** Supervision. **Yuefeng He:** Supervision, Funding acquisition.

Funding

This work was supported by the National Nature Science Foundation of China (Grant NO. 82160607), the Yunnan Fundamental Research Projects (Grant NO. 202401AT070177), Scientific and technological innovation team of environmental and occupational arsenic exposure carcinogenesis research of Kunming Medical University (CXTD202201), the Innovative Research Team of Yunnan Province (202405AS350016)

Declaration of Competing Interest

The authors declare that they have no known competing financial interests or personal relationships that could have appeared to influence the work reported in this paper.

Acknowledgements

The authors would like to thank all the subjects participating in the present study.

Data availability

The authors do not have permission to share data.

References

Adams, J.M., Cory, S., 2017. The BCL-2 arbiters of apoptosis and their growing role as cancer targets. Cell Death Differ. 25 (1), 27–36. https://doi.org/10.1038/cdd.2017.161.

Adli, M., Baldwin, A.S., 2006. IKK-I/IKKε controls constitutive, cancer Cell-associated NF-κB activity via regulation of Ser-536 p65/RelA phosphorylation. J. Biol. Chem. 281 (37), 26976–26984. https://doi.org/10.1074/jbc.M603133200.

Ahn, K.S., Sethi, G., Chao, T.-H., et al., 2007. Salinosporamide a (NPI-0052) potentiates apoptosis, suppresses osteoclastogenesis, and inhibits invasion through down-modulation of NF-κB–regulated gene products. Blood 110 (7), 2286–2295. https://doi.org/10.1182/blood-2007-04-084996.

Ali, I., A. Wani, W., Saleem, K., et al., 2012. Thalidomide: a banned drug resurged into future anticancer drug. CURR DRUG THER 7 (1), 13–23. https://doi.org/10.2174/157488512800389164.

Ali, I., Alsehli, M., Scotti, L., et al., 2020. Progress in polymeric nano-medicines for theranostic cancer treatment. Polymers 12 (3). https://doi.org/10.3390/polym12030598.

Ali, I., Lone, M.N., Suhail, M., Mukhtar, S.D., Asnin, L., 2016. Advances in nanocarriers for anticancer drugs delivery. Curr. Med Chem. 23 (20), 2159–2187. https://doi.org/10.2174/0929867323666160405111152.

Ali, I., Wani, W.A., Saleem, K., et al., 2013. Syntheses, DNA Binding and Anticancer Profiles of L-Glutamic Acid Ligand and its Copper(II) and Ruthenium(III) Complexes. 9 (1):, 11–21. https://doi.org/10.2174/157340613804488297.

Beauchef, G., Bigot, N., Kypriotou, M., et al., 2012. The p65 subunit of NF-κB inhibits COL1A1 gene transcription in human dermal and scleroderma fibroblasts through its recruitment on promoter by protein interaction with transcriptional activators (c-Krox, Sp1, and Sp3). J. Biol. Chem. 287 (5), 3462–3478. https://doi.org/10.1074/jbc.M111.286443.

Bock, F.J., Tait, S.W.G., 2019. Mitochondria as multifaceted regulators of cell death. Nat. Rev. Mol. Cell Biol. 21 (2), 85–100. https://doi.org/10.1038/s41580-019-0173-8.

Buss, H., Dörrie, A., Schmitz, M.L., Hoffmann, E., Resch, K., Kracht, M., 2004. Constitutive and Interleukin-1-inducible phosphorylation of p65 NF-κB at serine 536 is mediated by multiple protein kinases including IκB kinase (IKK)-α, IKKβ, IKKε, TRAF family Member-associated (TANK)-binding kinase 1 (TBK1), and an unknown kinase and couples p65 to TATA-binding Protein-associated factor II31-mediated Interleukin-8 transcription. J. Biol. Chem. 279 (53), 55633–55643. https://doi.org/10.1074/jbc.M409825200.

Chen, L.-Y., Chen, L.-W., Peng, K.-T., et al., 2020. Sp3 transcription factor cooperates with the Kaposi's Sarcoma-Associated herpesvirus ORF50 protein to synergistically activate specific viral and cellular gene promoters. J. Virol. 94 (18). https://doi.org/10.1128/jvi.01143-20.

Chen, Q., Ma, K., Liu, X., et al., 2022. Truncated PARP1 mediates ADP-ribosylation of RNA polymerase III for apoptosis. Cell Discov. 8 (1). https://doi.org/10.1038/s41421-021-00355-1.

Chen, J., Zhang, W., Pan, C., Fan, J., Zhong, X., Tang, S., 2021. Glaucocalyxin a induces cell cycle arrest and apoptosis via inhibiting NF-κB/p65 signaling pathway in melanoma cells. Life Sci. 271. https://doi.org/10.1016/j.lfs.2021.119185.

Czabotar, P.E., Lessene, G., Strasser, A., Adams, J.M., 2013. Control of apoptosis by the BCL-2 protein family: implications for physiology and therapy. Nat. Rev. Mol. Cell Biol. 15 (1), 49–63. https://doi.org/10.1038/nrm3722.

Dai, X., Chen, C., Yang, Q., et al., 2018. Exosomal circRNA_100284 from arsenite-transformed cells, via microRNA-217 regulation of EZH2, is involved in the malignant transformation of human hepatic cells by accelerating the cell cycle and

promoting cell proliferation. Cell Death Dis. 9 (5). https://doi.org/10.1038/s41419-018-0485-1.
Dang, Y., Zhang, Y., Xu, L., et al., 2020. PUMA-mediated epithelial cell apoptosis promotes helicobacter pylori infection-mediated gastritis. Cell Death Dis. 11 (2). https://doi.org/10.1038/s41419-020-2339-x.
Du, W.W., Yang, W., Liu, E., Yang, Z., Dhaliwal, P., Yang, B.B., 2016. Foxo3 circular RNA retards cell cycle progression via forming ternary complexes with p21 and CDK2. Nucleic Acids Res. 44 (6), 2846–2858. https://doi.org/10.1093/nar/gkw027.
Fan, Y., Mao, R., Zhao, Y., et al., 2009. Tumor necrosis Factor-α induces RelA degradation via ubiquitination at lysine 195 to prevent excessive nuclear Factor-κB activation. J. Biol. Chem. 284 (43), 29290–29297. https://doi.org/10.1074/jbc.M109.018994.
Ghantous, A., Saikali, M., Rau, T., Gali-Muhtasib, H., Schneider-Stock, R., Darwiche, N., 2012. Inhibition of tumor promotion by parthenolide: epigenetic modulation of p21. Cancer Prev. Res. 5 (11), 1298–1309. https://doi.org/10.1158/1940-6207.Capr-12-0230.
Hansen, T.B., Jensen, T.I., Clausen, B.H., et al., 2013. Natural RNA circles function as efficient microRNA sponges. Nature 495 (7441), 384–388. https://doi.org/10.1038/nature11993.
Hochrainer, K., Racchumi, G., Anrather, J., 2013. Site-specific phosphorylation of the p65 protein subunit mediates selective gene expression by differential NF-κB and RNA polymerase II promoter recruitment. J. Biol. Chem. 288 (1), 285–293. https://doi.org/10.1074/jbc.M112.385625.
Hossain, M.T., Li, S., Reza, M.S., et al., 2022. Identification of circRNA biomarker for gastric cancer through integrated analysis. Front. Mol. Biosci. 9. https://doi.org/10.3389/fmolb.2022.857320.
Jeck, W.R., Sharpless, N.E., 2014. Detecting and characterizing circular RNAs. Nat. Biotechnol. 32 (5), 453–461. https://doi.org/10.1038/nbt.2890.
Ji, Y., Ni, C., Shen, Y., et al., 2024. ESRP1-mediated biogenesis of circPTPN12 inhibits hepatocellular carcinoma progression by PDLIM2/ NF-kappaB pathway. Mol. Cancer 23 (1), 143. https://doi.org/10.1186/s12943-024-02056-1.
Kale, J., Osterlund, E.J., Andrews, D.W., 2017. BCL-2 family proteins: changing partners in the dance towards death. Cell Death Differ. 25 (1), 65–80. https://doi.org/10.1038/cdd.2017.186.
Kojima, C., Ramirez, D.C., Tokar, E.J., et al., 2009. Requirement of arsenic biomethylation for oxidative DNA damage. JNCI J. Nat. Cancer Institute 101 (24), 1670–1681. https://doi.org/10.1093/jnci/djp414.
Kuo, C.-C., Balakrishnan, P., Gribble, M.O., et al., 2022. The association of arsenic exposure and arsenic metabolism with all-cause, cardiovascular and cancer mortality in the strong heart study. Environ. Int. 159. https://doi.org/10.1016/j.envint.2021.107029.
Lamm, S.H., Boroje, I.J., Ferdosi, H., Ahn, J., 2021. A review of low-dose arsenic risks and human cancers. Toxicology 456. https://doi.org/10.1016/j.tox.2021.152768.
Li, X., Chen, S., Wang, X., et al., 2022. The pivotal regulatory factor circBRWD1 inhibits arsenic exposure-induced lung cancer occurrence by binding mRNA and regulating its stability. Mol. Ther. Oncolytics 26, 399–412. https://doi.org/10.1016/j.omto.2022.08.006.
Li, M., Chen, H., Xia, L., et al., 2021. Circular RNA circSP3 promotes hepatocellular carcinoma growth by sponging microRNA-198 and upregulating cyclin-dependent kinase 4. Aging 13 (14), 18586–18605. https://doi.org/10.18632/aging.203303.
Li, Y., Shen, L., Xu, H., et al., 2011. Up-regulation of cyclin D1 by JNK1/c-Jun is involved in tumorigenesis of human embryo lung fibroblast cells induced by a low concentration of arsenite. Toxicol. Lett. 206 (2), 113–120. https://doi.org/10.1016/j.toxlet.2011.06.024.
Liu, S.-J., Li, Z.-Q., Wang, X.-Y., Liu, F., Xiao, Z.-M., Zhang, D.-C., 2021. lncRNA UCA1 induced by SP1 and SP3 forms a positive feedback loop to facilitate malignant phenotypes of colorectal cancer via targeting miR-495. Life Sci. 277. https://doi.org/10.1016/j.lfs.2021.119569.
Mao, Y., Zhou, Q., Wang, J., et al., 2022. CircP50 functions through the phosphorylation- and acetylation-activated p53 pathway to mediate inorganic arsenic-induced apoptosis in A549 cells. Environ. Sci. Pollut. Res. 29 (60), 91232–91240. https://doi.org/10.1007/s11356-022-22094-w.
Medda, N., De, S.K., Maiti, S., 2021. Different mechanisms of arsenic related signaling in cellular proliferation, apoptosis and neo-plastic transformation. Ecotoxicol. Environ. Saf. 208. https://doi.org/10.1016/j.ecoenv.2020.111752.
Minna, J.D., Putila, J.J., Guo, N.L., 2011. Association of arsenic exposure with lung cancer incidence rates in the United States. PLoS ONE 6 (10). https://doi.org/10.1371/journal.pone.0025886.
Naujokas, M.F., Anderson, B., Ahsan, H., et al., 2013. The broad scope of health effects from chronic arsenic exposure: update on a worldwide public health problem. Environ. Health Perspect. 121 (3), 295–302. https://doi.org/10.1289/ehp.1205875.
Park, Y.-h, Kim, D., Dai, J., Zhang, Z., 2015. Human bronchial epithelial BEAS-2B cells, an appropriate in vitro model to study heavy metals induced carcinogenesis. Toxicol. Appl. Pharmacol. 287 (3), 240–245. https://doi.org/10.1016/j.taap.2015.06.008.
Pullella, K., Kotsopoulos, J., 2020. Arsenic exposure and breast cancer risk: a Re-Evaluation of the literature. Nutrients 12 (11). https://doi.org/10.3390/nu12113305.
Safe, S., 2023. Specificity proteins (Sp) and cancer. Int. J. Mol. Sci. 24 (6). https://doi.org/10.3390/ijms24065164.
Salmeri, N., Villanacci, R., Ottolina, J., et al., 2020. Maternal arsenic exposure and gestational diabetes: a systematic review and Meta-Analysis. Nutrients 12 (10). https://doi.org/10.3390/nu12103094.
Singh, R., Letai, A., Sarosiek, K., 2019. Regulation of apoptosis in health and disease: the balancing act of BCL-2 family proteins. Nat. Rev. Mol. Cell Biol. 20 (3), 175–193. https://doi.org/10.1038/s41580-018-0089-8.
Sun, X., Cao, S., Mao, C., Sun, F., Zhang, X., Song, Y., 2024. Post-translational modifications of p65: state of the art. Front. Cell Dev. Biol. 12. https://doi.org/10.3389/fcell.2024.1417502.
Takada, Y., Andreeff, M., Aggarwal, B.B., 2005. Indole-3-carbinol suppresses NF-κB and IκBα kinase activation, causing inhibition of expression of NF-κB-regulated antiapoptotic and metastatic gene products and enhancement of apoptosis in myeloid and leukemia cells. Blood 106 (2), 641–649. https://doi.org/10.1182/blood-2004-12-4589.
Tan, J., Sun, M., Luo, Q., et al., 2020. Arsenic exposure increased expression of HOTAIR and LincRNA-p21 in vivo and vitro. Environ. Sci. Pollut. Res. 28 (1), 587–596. https://doi.org/10.1007/s11356-020-10487-8.
Tan, J., Sun, M., Yin, J., et al., 2022. Hsa_circ_0005050 interacts with ILF3 and affects cell apoptosis and proliferation by disrupting the balance between p53 and p65. Chem. Biol. Interact. 368. https://doi.org/10.1016/j.cbi.2022.110208.
Viatour, P., Merville, M.-P., Bours, V., Chariot, A., 2005. Phosphorylation of NF-κB and IκB proteins: implications in cancer and inflammation. Trends Biochem. Sci. 30 (1), 43–52. https://doi.org/10.1016/j.tibs.2004.11.009.
Wang, X., Chen, M., Fang, L., 2021. hsa_circ_0068631 promotes breast cancer progression through c-Myc by binding to EIF4A3. Mol. Ther. Nucleic Acids 26, 122–134. https://doi.org/10.1016/j.omtn.2021.07.003.
Wang, H., Zhu, Y., Xu, X., et al., 2016. Ctenopharyngodon idella NF-κB subunit p65 modulates the transcription of IκBα in CIK cells. Fish. Shellfish Immunol. 54, 564–572. https://doi.org/10.1016/j.fsi.2016.04.132.
Wu, F., Chen, Y., Navas-Acien, A., Garabedian, M.L., Coates, J., Newman, J.D., 2021. Arsenic exposure, arsenic metabolism, and glycemia: results from a clinical population in New York city. Int. J. Environ. Res. Public Health 18 (7). https://doi.org/10.3390/ijerph18073749.
Xiao, T., Xue, J., Shi, M., et al., 2018. Circ008913,viamiR-889 regulation of DAB2IP/ZEB1, is involved in the arsenite-induced acquisition of CSC-like properties by human keratinocytes in carcinogenesis. Metallomics 10 (9), 1328–1338. https://doi.org/10.1039/c8mt00207j.
Xue, J., Liu, Y., Luo, F., et al., 2017. Circ100284, via miR-217 regulation of EZH2, is involved in the arsenite-accelerated cell cycle of human keratinocytes in carcinogenesis. Biochim. Et. Biophys. Acta Mol. Basis Dis. 1863 (3), 753–763. https://doi.org/10.1016/j.bbadis.2016.12.018.
Yang, Y., Gao, X., Zhang, M., et al., 2018. Novel role of FBXW7 circular RNA in repressing glioma tumorigenesis. JNCI J. Nat. Cancer Institute 110 (3), 304–315. https://doi.org/10.1093/jnci/djx166.
Yang, F., Tang, E., Guan, K., Wang, C.-Y., 2003. IKKβ plays an essential role in the phosphorylation of RelA/p65 on serine 536 induced by lipopolysaccharide. J. Immunol. 170 (11), 5630–5635. https://doi.org/10.4049/jimmunol.170.11.5630.
Yin, J., Zhou, Q., Tan, J., Che, W., He, Y., 2022. Inorganic arsenic induces MDM2, p53, and their phosphorylation and affects the MDM2/p53 complex in vitro. Environ. Sci. Pollut. Res. 29 (58), 88078–88088. https://doi.org/10.1007/s11356-022-21986-1.
Zhang, M., Huang, N., Yang, X., et al., 2018. A novel protein encoded by the circular form of the SHPRH gene suppresses glioma tumorigenesis. Oncogene 37 (13), 1805–1814. https://doi.org/10.1038/s41388-017-0019-9.
Zheng, Y., Mao, Y.-F., Zhao, H.-J., et al., 2021. Importance of monitoring arsenic methylation metabolism in acute promyelocytic leukemia patients receiving the treatment of arsenic trioxide. Exp. Hematol. Oncol. 10 (1). https://doi.org/10.1186/s40164-021-00205-6.